Available online at www.sciencedirect.com
ScienceDirect
International Journal of Heat and Mass Transfer 50 (2007) 283–291
International Journal of HEAT and MASS TRANSFER
www.elsevier.com/locate/ijhmt

A Photographic study of subcooled flow boiling burnout at high heat flux and velocity

G.P. Celata [a,*], M. Cumo [b], D. Gallo [c], A. Mariani [a], G. Zummo [a]

[a] *ENEA, National Institute of Thermal-Fluid Dynamics, Via Anguillarese 301, 00060 S.M. Galeria, Rome, Italy*
[b] *University of Rome, La Sapienza, DINCE, Corso Vittorio Emanuele, 244 – Rome, Italy*
[c] *Department of Nuclear Engineering, University of Palermo, Viale del Parco d'Orleans – Palermo, Italy*

Received 2 December 2005
Available online 22 August 2006

Abstract

The present paper reports the results of a visualization study of the burnout in subcooled flow boiling of water, with square cross section annular geometry (formed by a central heater rod contained in a duct characterized by a square cross section). The coolant velocity is in the range 3–10 m/s. High speed movies of flow pattern in subcooled flow boiling of water from the onset of nucleate boiling up to physical burnout of the heater are recorded. From video images (single frames taken with a stroboscope light and an exposure time of 1 μs), the following general behaviour of vapour bubbles was observed: when the rate of bubble generation is increasing, with bubbles growing in the superheated layer close to the heating wall, their coalescence produces a type of elongated bubble called vapour blanket. One of the main features of the vapour blanket is that it is rooted to the nucleation site on the heated surface. Bubble dimensions are given as a function of thermal-hydraulic tested conditions for the whole range of velocity until the burnout region. A qualitative analysis of the behaviour of four stainless steel heater wires with different macroscopic surface finishes is also presented, showing the importance of this parameter on the dynamics of the bubbles and on the critical heat flux.

1. Introduction

Over the last 40 years, the interest of researchers toward boiling crisis and the relative critical heat flux (CHF) in subcooled flow boiling of water, has been increasing initially due to the development of nuclear fission reactors and recently to thermonuclear fusion reactor requirements. Subcooled flow boiling is a very efficient heat transfer regime for the cooling of those components which are subjected to very high heat fluxes, where the CHF, with the associate burnout of the heat transfer surface, represents an insurmountable limit for this efficient heat transfer technique.

Although the interest for CHF is high, a detailed knowledge of the phenomena causing the boiling crisis on the heat transfer surface is scarce, and, in particular, there are still relevant disagreements, among researchers, about the mechanisms triggering the boiling crisis. Disagreements are caused by the fact that the direct observation of the heater surface during the boiling crisis, by means of flow visualization, is very difficult because of small vapour bubble dimensions, bubble crowding and high liquid velocity. Therefore, relatively few works on burnout visualization were carried out in the past, and, in particular very few of them reported direct observations of the boiling phenomena at the CHF, [1,2,4–8].

From the few experimental works available on flow visualization at the CHF, it is not possible to get a clear insight into the boiling crisis mechanisms. In particular, the lack of direct observations of boiling phenomena correlated, and the limited measurements of bubble parameters and wall temperature excursions does not allow the clarification of the actual event sequence for increasing heat flux values up to the CHF.

The objective of the present work is to perform a photographic study of the burnout in highly subcooled flow

* Corresponding author. Tel.: +39 6 30483905; fax: +39 6 30483926.
E-mail address: celata@casaccia.enea.it (G.P. Celata).

0017-9310/$ - see front matter © 2006 Elsevier Ltd. All rights reserved.
doi:10.1016/j.ijheatmasstransfer.2006.06.020

Nomenclature

CHF	critical heat flux, kW/m^2
D_B	vapour bubble diameter or height, μm
d_p	diameter of corundum grain, μm
L_B	vapour bubble width, μm
ONB	onset of nucleate boiling
p	pressure, MPa
q''	heat flux, kW/m^2
q''_{CHF}	critical heat flux, kW/m^2
r^*	critical size of a cavity, m, Eq. (1)
T_{in}	inlet temperature, °C
T_{sat}	saturation temperature, °C, Eq. (1)
T_w	wall temperature, °C, Eq. (1)
u	velocity, m/s
W_{th}	thermal power, kW
$\Delta T_{sub,in}$	inlet subcooling, K
λ	latent heat of vaporization, J/kg, Eq. (1)
ρ_G, ρ_L	vapour and liquid density, kg/m^3, Eq. (1)
σ	surface tension, N/m, Eq. (1)

boiling, in order to provide a quantitative description of the flow pattern under different conditions of the boiling regime. In addition, results of vapour bubble parameter measurements will be provided for all boiling regimes, especially during the boiling crisis. A qualitative analysis of the behaviour of four stainless steel heater wires with different macroscopic surface finishes is also presented, showing the importance of this parameter on the dynamics of the bubbles and on the critical heat flux.

2. Experimental apparatus and test procedure

The high speed photographic study of burnout in subcooled flow boiling of water has been performed using the water loop shown in Fig. 1, while the test section is schematically drawn in Fig. 2.

The loop, made of Type 304 stainless steel and filled with deionized water, consists of the following components: main alternative pump, damper, filter, turbine flow meter, heated test section and water cooled tank. The test section is vertically oriented with water flowing upwards. It has been designed to obtain images of the flow boiling, over the surface of the heater, using a transmission method of illumination.

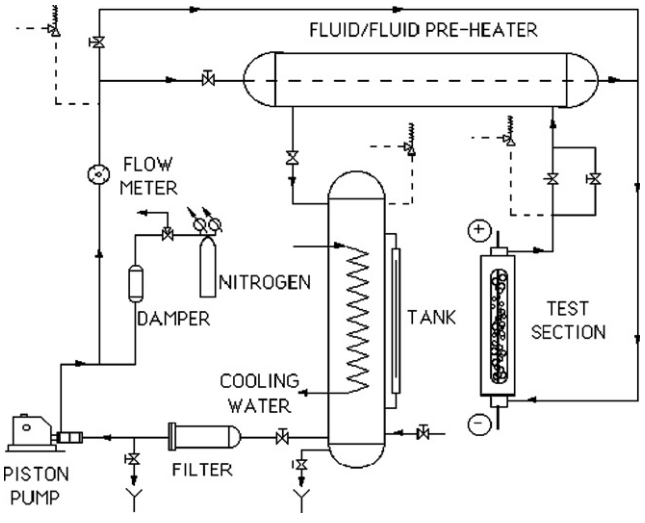

Fig. 1. Schematic diagram of the experimental facility.

The test section consists of two parts: the casing and the heater. In the casing we have a square duct flow channel. Two out of the four walls of the flow channel in the casing are made of Plexiglas, so that the light passes through these two transparent plates and illuminates the surface of the heater on which the boiling phenomena occur. The annulus has a square duct, the walls of which are respectively the two plates of Plexiglas and two stainless steel walls of the test section body, with a cylindrical heater (solid rod) at the center of the square duct. The side dimension of the square duct is 7.2 mm.

Dimensions of the cylindrical heater are 2 mm in diameter and 100 mm in length. The heater, one for each run, is made of stainless steel 316L Type, and is uniformly heated over its length by Joule effect using an electric feeder, which is up to 90 kW (50 V).

The bulk fluid temperature is measured just upstream and downstream of the test section using 0.5 mm K-type thermocouples, error ±0.5 °C. The downstream thermocouple is located after suitable mixing of the fluid is achieved in order to ensure full condensation of all bubbles and therefore uniform temperature distribution. This makes the bulk exit temperature suitable for an energy balance in the fluid. The knowledge of the inlet and outlet temperatures, together with the measurement of the water mass flow rate, error ±1%, allows the evaluation of the heat balance in the coolant (calorimetric method), i.e., the calculation of the thermal power delivered to the fluid, error ±4%. Thus there is no need to calculate heat losses from the test section. All the parameters are continuously monitored using digital and analogue displays, and each variation is recorded. The experimental procedure consists in the following series of actions: the mass flow rate is set up using a manual control of the piston pump. Once the flow rate is steady, the thermal power is delivered to the test section. The control parameter used while approaching the CHF is the electrical power delivered to the test section, and the initial step in the thermal power is 0.5 kW. Once 70% of the expected CHF value is reached, the increment is reduced to 0.1 kW (from 0.1% to 0.6% of the CHF). The expected CHF value is evaluated by previous

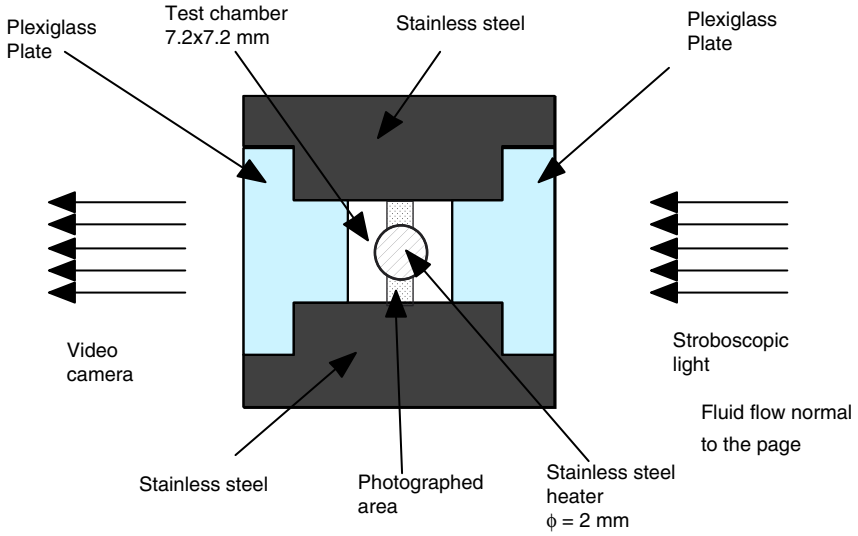

Fig. 2. Test section (not to scale).

experiments in channels with similar geometric conditions and same inlet conditions of the coolant. After each step, small adjustments in the flow rate are made, so that the exit flow conditions correspond to the desired ones. The above reported procedure is repeated until burnout occurs. The burnout is evidenced by the heater destruction and is detected by the sharp drop in the electrical power reading.

The visualization of the burnout was performed using the optical arrangement shown in Fig. 2. Obtaining images of the burnout in subcooled flow boiling of water is complicated by various factors, such as the small size of vapour bubbles (<0.1 mm), the high flow velocity (up to 10 m/s), the difficulty in defining the exact position of the burnout along the heater, associated with the very small portion of the heater intersected by the light transmission due to the large image magnification required, and the impossibility to define the exact instant of occurrence of the burnout. In order to get good pictures of bubbles at a velocity of about 10 m/s and with size of some tens of micron, it is necessary to have an exposure time no longer than 1 μs. With regard to earlier works [1,2], the optical bench has been completely changed in the light source and in the camera, in order to have more light and improve the pictures. A Kodak MAS STROBE stroboflash has been used as a light source, coupled with a CCD PCO Flashcam. The camera is equipped with a shutter of 1 μs, while the stroboflash has a flash length of about at 20 μs. It has been necessary to design and arrange an electronic interface capable of synchronizing the peak flashlight with the camera openings. Due to the random nature of boiling, the relevant parameters of the vapour blanket (i.e., elongated bubbles due to small bubbles coalescence) are measured from the video images based on the following arguments. Images consist of a sequence of frames spaced apart 20 ms. As the boiling cycle of a single vapour bubble lasts for less than 20 ms, and as active microcavities have variable waiting periods, each frame shows the situation of the heater surface in a random instant of the boiling cycle. The dimensions of the largest vapour bubbles present in the frames are measured. In this way, it is reasonable to consider that the measured dimensions of the bubbles represent the maximum sizes that can be reached under those conditions. The values reported in graphs are the average among measurements obtained from different images at the same heat flux. This aspect, also, minimizes the effect of the 2-D image of the pictures. The images of burnout are analysed through a PC digital image processing system. The error on bubble size is constant and equal to 11 μm.

3. Experimental results

A summary of the test conditions (liquid velocity, system pressure and inlet temperature) for the present experimental campaign is given in Table 1 for the tests with the same superficial finish. The inlet temperature for the tests with the screwed and the sandblasted surface is $T_{in} = 20$ °C, the velocity and pressure are, respectively, 3 m/s 0.5 MPa, 3 m/s 1.0 MPa, 3 m/s 2.0 MPa, 10 m/s 2.0 MPa. The run with the test section treated with an electrolytical system is done with 3 m/s and 1.0 MPa. The sandblasted test section was made as follows: the heater was polished until there were no cavities, then it was sandblasted with very fine corundum grain ($d_p = 25$ μm), with a pressure of $p = 1$ bar. The average surface roughness is about 0.16 μm, as evaluated from a measurement with a profilometer (error 10%).

Table 1
Test conditions (the value reported is the inlet temperature)

u (m/s)/p (MPa)	0.5 (°C)	1.0 (°C)	2.0 (°C)	3.0 (°C)
3.0	20	20–40–60	20	20
5.0	20	20	20–40–60	20
7.5		20	20	20
10.0			20	20

3.1. Wall temperature measurement

The heater wall temperature is obtained from the change in length of the heater rod for each heat flux step. A schematic of the heater length measurement system is drawn in Fig. 3. The heater rod is formed by three components: lower copper clamp, stainless steel (AISI 316L) rod and upper copper clamp. From the knowledge of the thermal properties of AISI 316L and copper it is possible to evaluate the mean temperature of the stainless steel rod. The wall temperature is calculated using the conduction Fourier's law:

$$\frac{d^2T}{dr^2}+\frac{1}{r}\frac{dT}{dr}+\frac{q}{k}=0$$

with boundary conditions:

$$T = T_w \quad \text{at } r = R$$

$$Q\pi R^2 L = -2\pi kRL(dT/dr) \quad \text{at } r = R$$

The average temperature is obtained by integration and is:

$$T_{w,a} = T - (qR^2/6k)$$

The wall temperature obtained with this procedure is the mean value of the heater surface temperatures in the heated section (error ±5% obtained from a calibration with glycerol and a thermometer). Nonetheless, once subcooled flow boiling spreads all along the channel, the heater temperature is almost uniform, and its approximation with the average value obtained from the experimental apparatus would seem to be quite reasonable.

The aim of the wall temperature measurement is to record this parameter and to correlate the information directly to the heat transfer and flow regime. Fig. 4 shows one typical test for which the measured wall temperature is reported versus the heat flux, together with the bubble width, L_B and height D_B, (or diameter, if we suppose the bubble as spherical), as obtained from the pictures. The definition of these parameters is given in Fig. 5. The trend of the three parameters is similar to that of the previous findings, confirming conclusions made in Celata et al. [1,2].

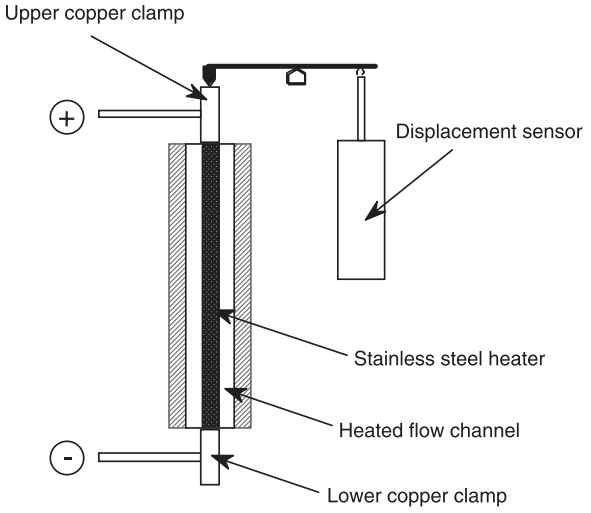

Fig. 3. Schematic representation of the heater elongation measurement system.

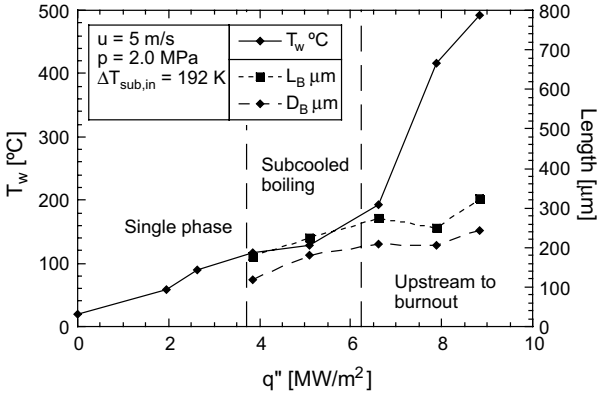

Fig. 4. Measured wall temperature and vapour bubble width and height versus heat flux.

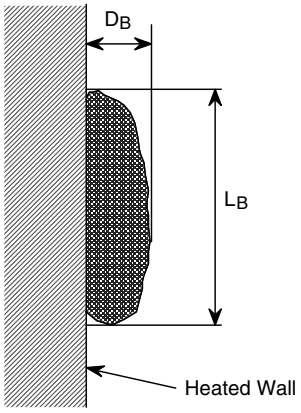

Fig. 5. Definition of vapour bubble parameters.

After the onset of nucleate boiling (ONB), the regime changes from a microbubble regime close to the heated wall to isolated bubbles. As the heat flux increases, bubble coalescence takes place up to the occurrence of hot spots on the heated wall and the final phase where the boiling activity is very reduced, before the physical burnout is experienced. The wall temperature curve is characterized by three zones with a different slope, corresponding to single-phase flow, subcooled boiling and upstream burnout.

In this section, we will report on the trends of the bubble sizes as a function of the thermal hydraulic parameters (inlet subcooling, water velocity and heat flux) where these parameters were varied. Though the best situation would be represented by a single parameter variation, other conditions being equal, this has not always been possible in present tests. The effect of the pressure is described jointly with the subcooling effect. Only one surface finish (extruded stainless steel) was used in the tests described in this section.

3.1.1. Pressure and/or inlet subcooling effect

Pressure and inlet subcooling effect are strictly interrelated, because due to the complexity of tests, we carried out tests with different pressures and constant water inlet temperatures, thus having different inlet subcooling for each test. The subcooling effect, at constant pressure, has been studied in some tests where only the water inlet temperature has been varied, while other conditions (velocity and pressure) were kept constant. The width of the bubble L_B is reported in Fig. 6a as a function of the heat flux, while, similarly, Fig. 6b shows the trend of the bubble height, D_B. The three tests reported in Fig. 6 refer to three different water inlet temperatures and, since the pressure was constant, to three different degrees of subcooling. The effect of degree of subcooling is as expected, i.e., bubble dimensions, L_B and D_B increase as the degree of subcooling decreases, for a given heat flux. They both increase with the heat flux if other conditions are equal. The highest heat flux for each series at a given degree of subcooling is the critical heat flux. The width of the bubble, L_B, ranged between 200 μm and 1 mm, while the height, D_B, was found to be between 150 and 340 μm. Bubbles are therefore very flat and stretched along the heating wire surface. It is worthwhile to mention here that after each test (which is destructive, requiring the substitution of the heating wire) we observed a considerable oxidation of the heating surface due to the heating of the wire before reaching the burnout condition.

Fig. 7 shows bubble sizes as a function of the ratio between the heat flux delivered to the fluid and the critical heat flux, with the inlet pressure as one of the parameters that were varied. In this case, water velocity and inlet temperature were kept constant, thus providing different inlet degree of subcooling of the water. Although in this case we have an effect of the subcooling added to that of the pressure, it is interesting to draw some remarks. The observed trend is as expected, i.e., bubble sizes are larger for the lower pressure, apart from some uncertainty for the low heat flux, easily explainable with the steam specific volume variation with the pressure. As the heat flux approaches the critical heat flux, in most cases the height of the bubble tends to decrease or to remain constant with an increase in the heat flux, as shown by the flattening of the curves. As already said above and in Celata et al. [2], when approaching the burnout, the boiling activity is reduced, sometimes drastically, before reaching the physical destruction of the wall. We repeated some tests to check the reproducibility of the results. In spite of the fact that

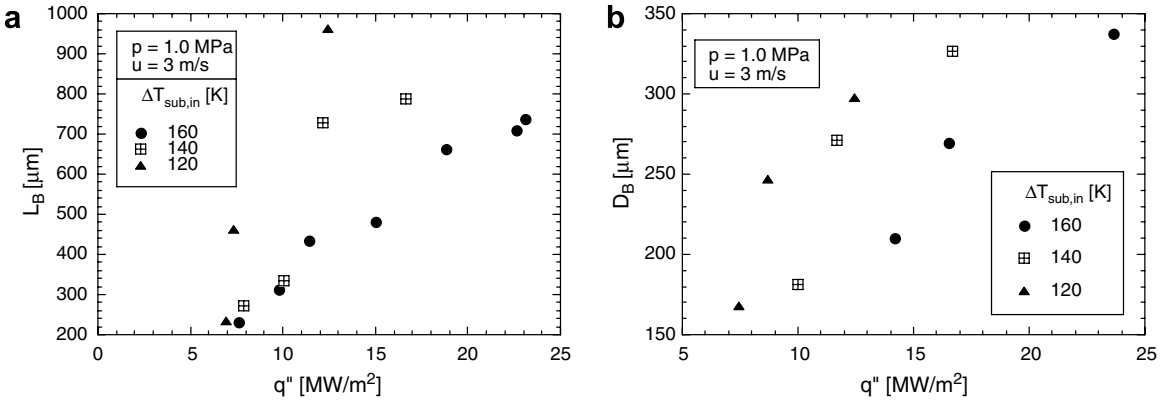

Fig. 6. Influence of inlet subcooling on the bubble width, L_B and height, D_B.

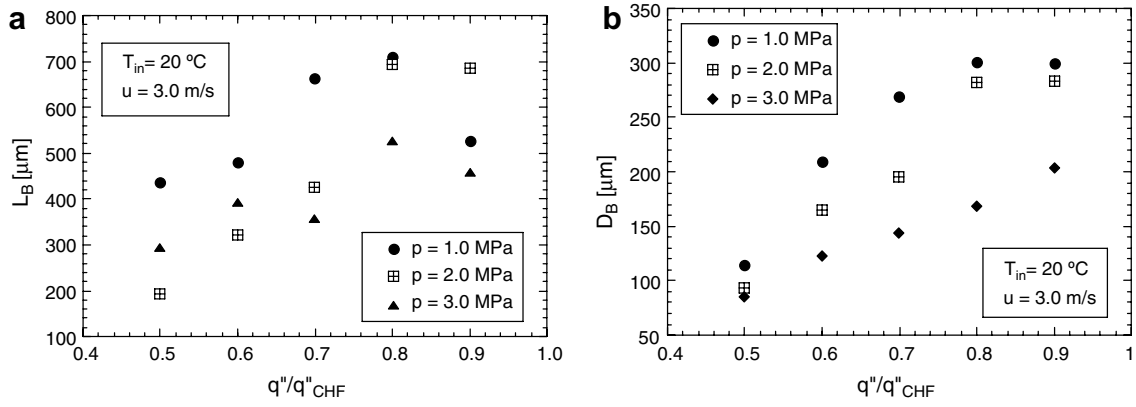

Fig. 7. Influence of exit pressure on bubble sizes.

test section was changed in each test, very narrow scatter has been found in repeated tests thus showing a good reproducibility of data.

Another representation of bubble sizes is plotted in Fig. 8, where D_B and L_B are plotted versus the water inlet degree of subcooling for different values of the ratio q''/q''_{CHF}, and for fixed values of the water inlet temperature and velocity. The variation in the water subcooling is obtained by changing the system pressure. The bubble height D_B exhibits an almost linear trend with the degree of subcooling, the slope of which tends to increase with the heat flux.

Also in this case, as already observed in Fig. 7, when the heat flux is close to the CHF (the $q''/q''_{CHF} = 0.9$ groups values ranging from 0.9 to 0.98) the height of the bubble remains constant or decreases. An inverse dependence on

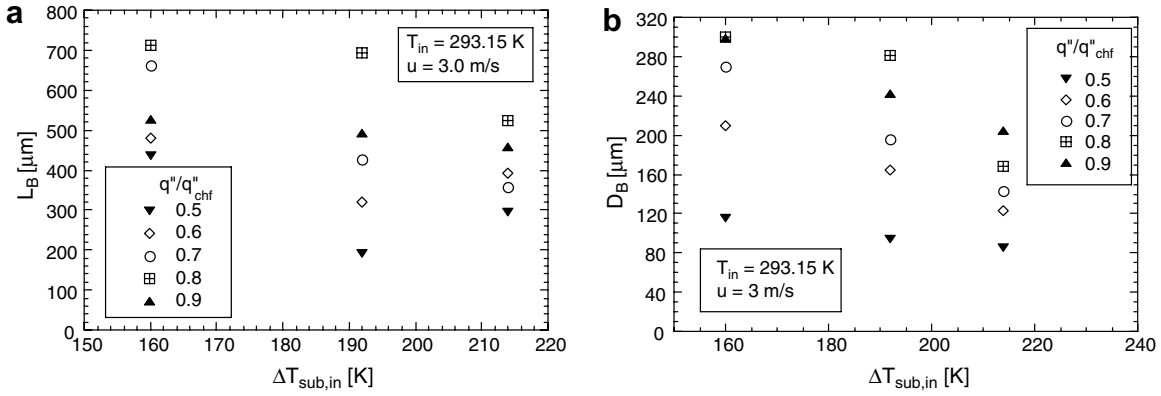

Fig. 8. Influence of subcooling on bubble sizes.

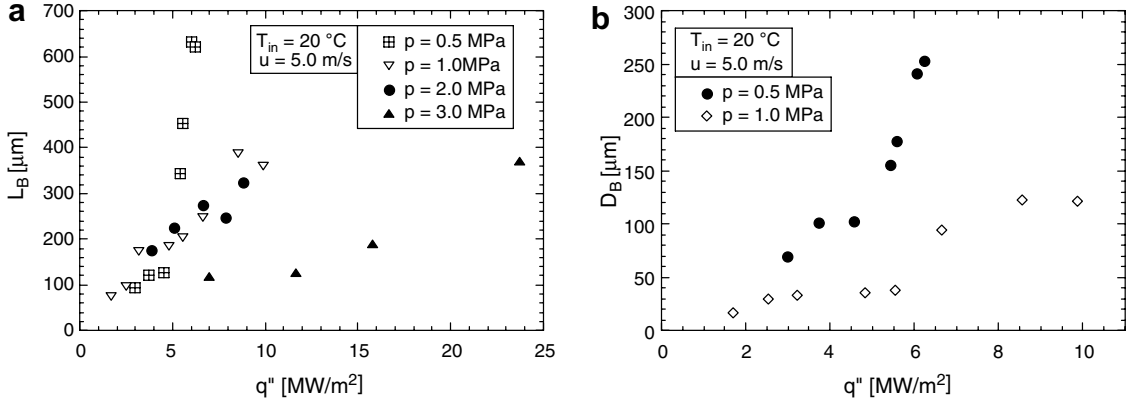

Fig. 9. Influence of exit pressure on bubble sizes.

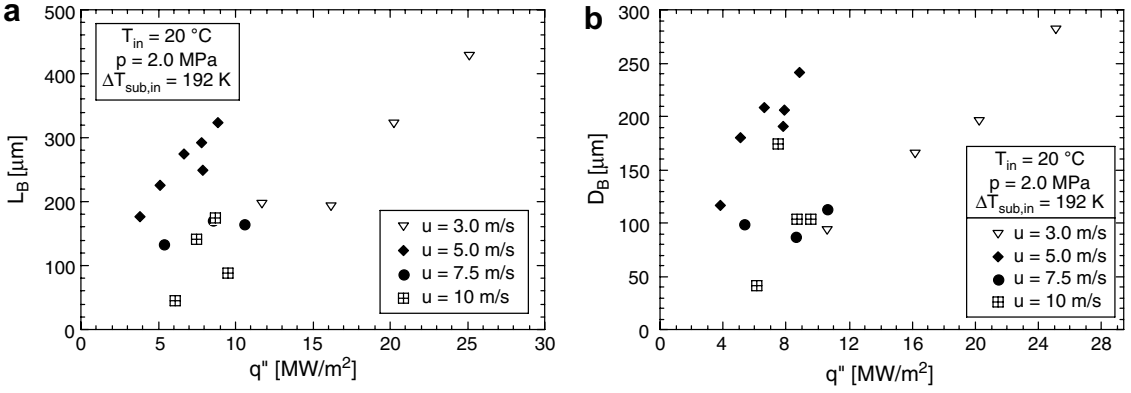

Fig. 10. Influence of liquid velocity on bubble sizes.

degree of subcooling is also demonstrated by L_B, although the linearity cannot be observed, conclusion on these trends are difficult since there are only three points.

Fig. 9 reports bubble sizes versus the heat flux, with the pressure as a parameter, for given values of the water inlet temperature and velocity. The change of the slope in the trend of D_B and L_B versus the heat flux is also quite clear from this representation.

Of course, figures reported in the manuscript are only samples of the many pictures taken during the experimental campaign. Conclusions refer to all pictures.

3.1.2. Effect of water velocity

Another parameter having an important effect on bubble dimensions is the water velocity in the test channel. As all the tests are carried out in the subcooled boiling regime with many bubbles still adherent to the heating wall, the higher velocity can either elongate the bubble or cause early detachment from the wall (this latter event has been observed at 10 m/s).

Fig. 10 shows bubble sizes, L_B and D_B, versus the heat flux, for different of fluid velocities, other conditions being equal. Trends are increasing functions of the heat flux, while the dependence of D_B and L_B, on water velocity is inverse, i.e., the higher the velocity the smaller the D_B and L_B are. The larger scattering of data for the highest velocity is due to the smaller number of bubbles present in each picture and to their smaller size. This causes a measurement which is statistically worse, while the error in the bubble size measurement is higher for smaller bubbles, in percent, as it is based on the same calibration of the digital image system and is therefore constant in the absolute value.

3.2. Analysis of the surface finish effect on the subcooled boiling and on the CHF

The surface finish of the heating wall may greatly affect nucleation boiling, and therefore the CHF, as bubble nucleation and growth mainly occurs because of the cavities on the wall surface. Further, the cavity size is also important, as only cavities above a given size (depending mainly on the surface tension of the fluid) are active for nucleation for a given heat flux. Specifically, Cumo [3] found that for each wall superheating, $T_w - T_{sat}$, there is a specific critical size r^*, and that only those cavities having an average size of r^* will become active centers for bubble formation. The relationship correlating r^* with the wall superheat is given by:

$$r^* = \frac{2\sigma T_{sat}\left(\frac{1}{\rho_G} - \frac{1}{\rho_L}\right)}{\lambda(T_w - T_{sat})} \quad (1)$$

This is also in agreement with Thorncroft et al. [9]). These authors proposed a model for the calculation of minimum and maximum cavity radius for nucleation in flow boiling. They found that in flow boiling, the ratio r_{max}/r_{min} is reduced to the unity, and the active nucleation sites characterized by cavity radius larger than r_{min} become deactivated. This phenomena is due to the increase of bulk turbulence, which causes a reduction of thermal boundary layer thickness on the heated surface. Having introduced the scheme we can specify the reference conditions of the heating wires used in the present tests. Those used in the

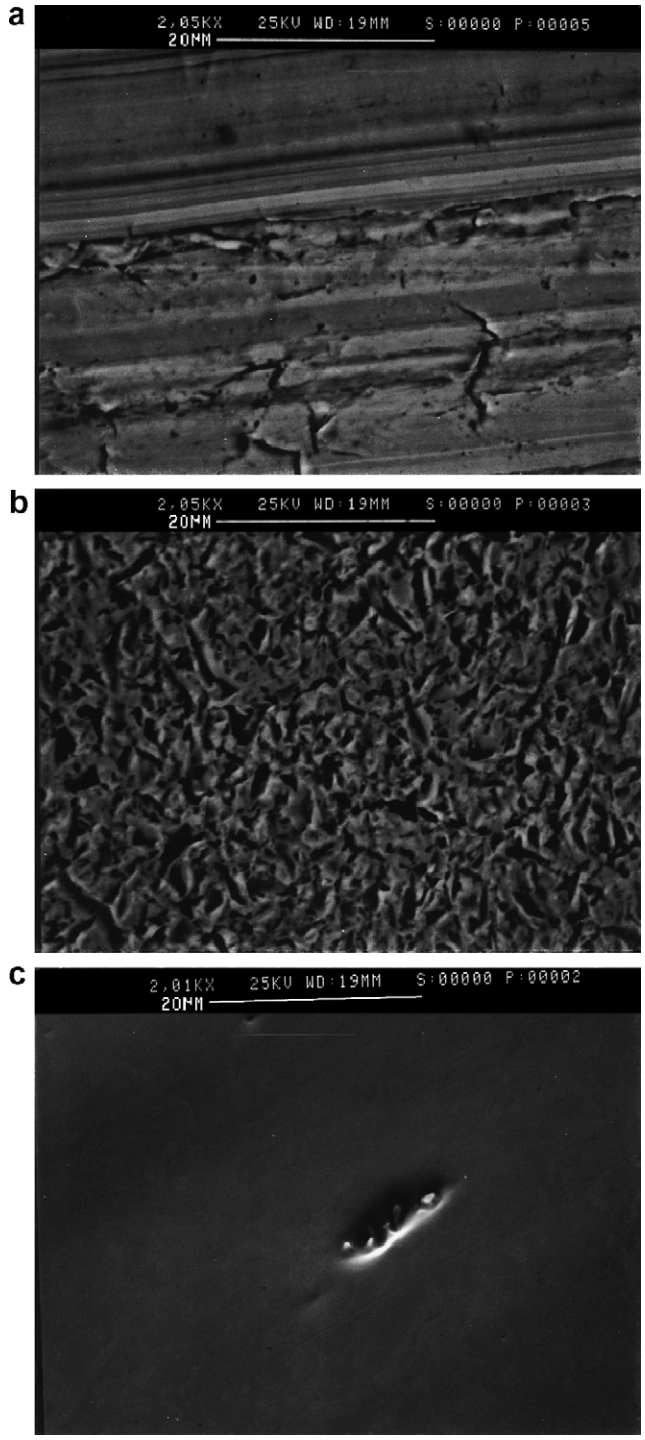

Fig. 11. Pictures of the different surface finish obtained with an electronic microscope: (a) normal wire (2050×), (b) sandblasted wire (2050×), (c) electrolytically treated wire (2010×).

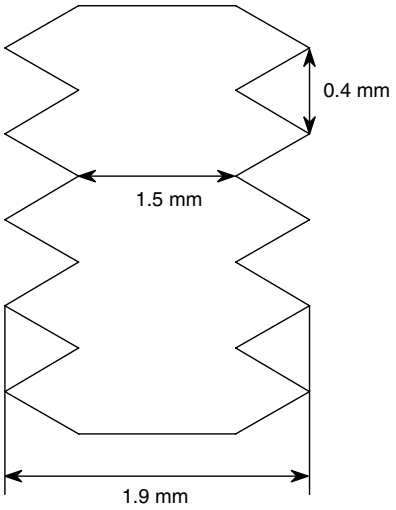

Fig. 12. Threaded test section. Schematic.

tests described above are made of extruded stainless steel and are not treated on the surface. A picture of the surface taken with the electronic microscope, Fig. 11a at 2050×, shows cavities of different sizes, striations and bosses in the longitudinal direction. This type of surface can permit nucleation with a wide range of wall superheat as, on average, the spectrum of the cavity average radius is very wide.

The second type of heating wire used is the same wire as above, threaded on the surface, and therefore macroscopically much different. These wires have a peak-to-peak distance of about 0.4 mm, as shown in the schematic of Fig. 12.

A third type of heating wire was obtained polishing the surface of the wire until there were no cavities. The surface was sandblasted with very fine corundum grain (d_p about 25 μm) at a pressure of 1 bar. The result is shown in Fig. 11b, where a 2050× picture taken with the electronic microscope exhibits a more uniform distribution of cavities.

The fourth type of surface finish has been obtained by sinking the wire in an orthophosphoric acid which contained glycerol and nigrosine, and treated in an electrolytic process as an anode. The 2010× picture reported in Fig. 11c shows a very smooth surface, practically without cavities, apart from a central point.

The treated surfaces have all been obtained starting from the same wires used in tests described above.

Typical results of the tests with different surface finish conditions are reported in Fig. 13, where, again, bubble sizes, L_B and D_B are plotted versus the heat flux to critical heat flux ratio for different types of wire.

Looking at the L_B trend we can see the regular, almost linear increase in L_B with the heat flux (referred to the CHF). The threaded wire shows a lower L_B than the normal wire until $q'' = 0.6q''_{CHF}$, which is the condition for which the bubble leaves the groove between two adjacent threads. If we remember that the distance between the bottom of the groove and the top of the thread is around 0.2 mm, we realize from the D_B curve in Fig. 13 that at around 60% of the CHF, the bubble height is of the same order of magnitude of the groove and the bubbles can detach towards adjacent grooves. For lower values of the heat flux the bubble is constrained in the groove and cannot grow in the axial direction. This may explain the lower L_B values for the threaded wire with respect to the normal one. Once the bubble leaves the groove, the L_B value suddenly jumps to values typical of the normal wire. The width of the bubble at the CHF is quite the same in the two cases, being governed by the Helmholtz instability.

The behaviour of the sandblasted and electrolytically treated wires, in terms of L_B, is quite similar. The bubble width is much shorter than that for the normal wire (and slightly shorter for the electrolytically treated wire, which provides a smoother surface, than the sandblasted wire), with the first bubble appearing only for a heat flux around 60–70% of the CHF. A very reduced population of bubbles was observed, with respect to the normal wire, for both the sandblasted and electrolytically treated wires.

As far as the trend of the bubble height versus the heat flux (referred to the CHF) is concerned, we can see from Fig. 13 that the threaded wire shows the highest value of D_B. This is also due to the above mentioned constraints of the bubble inside the groove. As the bubble cannot grow along the wire until it leaves the groove, the vapour

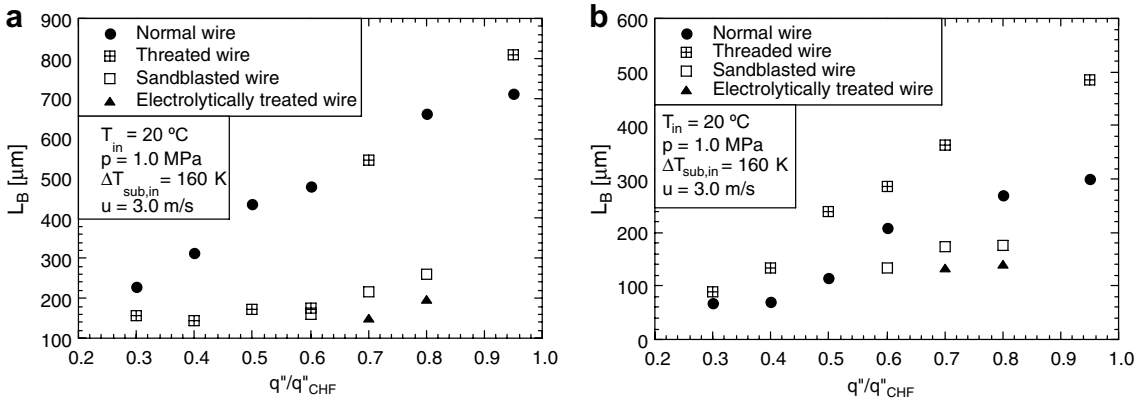

Fig. 13. Influence of surface finish on bubble sizes.

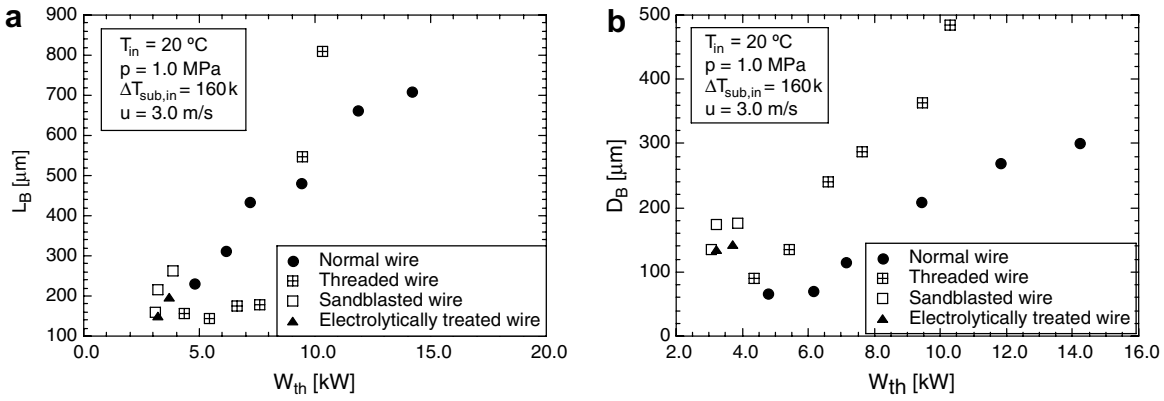

Fig. 14. Influence of surface finish on bubble sizes.

produced inside the groove itself will contribute to the increase of the bubble height. Similarly to L_B, the D_B for the sandblasted and electrolytically treated wires is much smaller than the normal wire. Fig. 14 shows the same data plotted versus the total thermal power delivered to the fluid. We did not use the heat flux in view of the difficulty to define it for the threaded wire, respect to the smooth surfaces. In Fig. 13 the ratio between the heat flux and the critical heat flux is plotted. This is only an indication of the distance from thermal crisis conditions.

As we can see, the sandblasted and electrolytically treated wires, though starting the nucleation activity at a similar thermal power as the other wires, experience the occurring of the physical burnout very early, i.e., at a thermal power (or heat flux) which is about 28% of the burnout thermal power for the normal wire. Because for the very reduced nucleation, for the same thermal power we will have a higher superheating of the wall and thus an earlier occurrence of the physical burnout. Also the threaded wire shows a premature burnout with respect to the normal wire (about 25% less in the thermal power at the CHF).

4. Conclusions

An experimental study on the visualization of the boiling phenomena up to the CHF in subcooled boiling of water at high velocity is presented.

Main conclusion that can be stated are:

- characterization of bubble size as a function of the thermo-hydraulic parameters with the evaluation of bubble sizes, range from 0.2 to 1.0 mm and
- bubble sizes increase with the heat flux and decrease with an increase in the degree of subcooling the pressure and the velocity.

Tests conducted with heating wires characterized by a different surface finish have shown that bubble sizes are larger for a surface with a greater number of cavities and a wider spectrum of cavity size. Smoothed wires (sandblasted and electrolytically treated surfaces) have exhibited a premature burnout with respect to the normal wire, in view of the drastic reduction of bubble generation at the wall.

Acknowledgements

The authors wish to thank Prof. D. Gorenflo and Dr. A. Luke for their help in the treatment of sandblasted wires, Mr. L. Falzetti for his work in preparing the electrolytical treated wires and providing the electronic microscope pictures.

References

[1] G.P. Celata, M. Cumo, A. Mariani, G. Zummo, Preliminary remarks on visualization of high heat flux burnout in subcooled water flow boiling, in: G.P. Celata, R.K. Shah (Eds.), Two-Phase Flow Modelling and Experimentation, vol. 2, Edizioni ETS, 1995, pp. 859–872.
[2] G.P. Celata, M. Cumo, D. Gallo, A. Mariani, G. Zummo, Visual investigation of high heat flux burnout in subcooled flow boiling of water, in: Third International Conference on Multiphase Flow, ICMF'98, Lyon, France, June 8–12, 1998.
[3] M. Cumo, Aspetti fondamentali dell'ebollizione, CNEN report RT/ING(67)15, 1967 (in Italian).
[4] M.P. Fiori, A.E. Bergles, Model of critical heat flux in subcooled flow boiling, in: Fourth International Heat Transfer Conference, Paris–Versailles, vol. 4, B 6.3, 1970.
[5] F.C. Gunther, Photographic study of surface-boiling heat transfer to water with forced convection, Trans. ASME 73 (1951) 115–121.
[6] G.J. Kirby, R. Stainforth, J.H. Kinneir, A visual study of forced convection boiling. Part 1. Results for a flat vertical heater, Atomic Energy Establishment Winfrith, AEEW – R 281 (1965).
[7] G.J. Kirby, R. Stainforth, J.H. Kinneir, An investigation into a possible mechanism of subcooled burnout, Atomic Energy Establishment Winfrith, AEEW – M 725 (1967).
[8] G.J. Kirby, R. Stainforth, J.H. Kinneir, A visual study of forced convection boiling. Part 2. Flow patterns and burnout for a round test, Atomic Energy Establishment Winfrith, AEEW – R 506 (1967).
[9] G.E. Thorncroft, J.F. Klausner, R. Mei, Suppression of flow boiling nucleation, J. Heat Transfer 119 (1997) 517–524.